Electrochimica Acta 531 (2025) 146411

Contents lists available at ScienceDirect

Electrochimica Acta

journal homepage: www.journals.elsevier.com/electrochimica-acta

Following Zn corrosion during long term immersion test in physiological solutions to establish the potential of zinc as biodegradable prosthetic material

D. Pupillo [a], F. Di Franco [b,*], L. Iannucci [a], S. Grassini [a], S. Virtanen [c], M. Santamaria [b]

[a] Dipartimento di Scienza Applicata e Tecnologia, Politecnico di Torino, 10129 Torino, Italy
[b] Dipartimento di Ingegneria, Università degli Studi di Palermo, 90128 Palermo, Italy
[c] Department of Materials Science and Engineering, Friedrich-Alexander-Universität Erlangen-Nürnberg, 91058 Erlangen, Germany

ARTICLE INFO

Keywords:
Zinc
Biodegradable implants
Zinc corrosion mechanisms
Physiological solutions
Proteins

ABSTRACT

Corrosion behaviour of commercially pure Zn during immersion up to 4 weeks is studied in three different solutions mimicking physiological environment, i.e. Hanks' Balance Salt Solution (HBSS), Dulbecco's modified Eagles' medium (DMEM) and DMEM with 10 % of fetal bovine serum (DMEM + 10 % FBS). Morphological characterizations, electrochemical tests, weight loss, and ion release measurements show that the corrosion mechanism is significantly affected by the physiological solution. In HBSS a phosphate-based conversion layer forms resulting to significantly slow down the corrosion rate, while in DMEM an intergranular corrosion occurs. The latter is hindered due to the presence of proteins from the fetal bovine serum in DMEM+FBS. The main cathodic process is oxygen reduction in all physiological media. Direct estimate of corrosion rate by gravimetric measurements revealed that zinc dissolution becomes very slow after two weeks of immersion in the employed physiological thus suggesting that zinc is not suitable for the fabrication of biodegradable implants in static fluidic condition.

1. Introduction

Biodegradable metallic implants are proposed to replace permanent biomaterials, for applications where the implants are required only to stay in the host for the time of tissues healing, to avoid chronic inflammations, secondary surgery to remove the implant, stress shielding phenomena, and thrombosis [1–4].

Up to now, Mg-based alloys are the most studied as biodegradable materials, due to very low corrosion resistance, cytocompatibility and suitable mechanical properties. However, the corrosion resistance of Mg-based materials is too low, especially in chloride-containing environments (as in the body environment) and in presence of impurities or intermetallic phases within the matrix causing non-uniform corrosion. In addition, the generation and accumulation of H_2 gas by the cathodic reaction in Mg corrosion is of concern for safe applications [1,5–8]. More recently, pure iron and zinc-based materials have been proposed as good candidate for biodegradable implants [9–13]. However, the corrosion rate of iron is lower than that of the other suggested metals and the corrosion products are too stable in the human body, thus their application in biodegradable implants is still a challenge. Zinc, being one of the essential trace metals in human bodies, seems a promising candidate due to its adequate corrosion rate and oxygen reduction reaction (ORR) as the main cathodic process [4,14,15]. However, strength and ductility of as cast zinc are generally below the mechanical benchmark for biodegradable implants, such as bone fixtures and stents, but can be enhanced by adding alloying elements [16–19].

In the last decades, several papers have been published trying to study the corrosion mechanisms of zinc in human body [4,20–23], but some aspects remain unclear. Indeed, zinc oxidation and dissolution can be strongly influenced by the composition, temperature, and hydrodynamic conditions of the environment, thus the role of the employed electrolytic solution selected to mimic a physiological environment is very important. It is widely known that a key factor affecting the corrosion behaviour of zinc is chloride ion concentration, since Cl^- induces localized corrosion. However, a role is also played by the other compounds present in the electrolyte considering the complex nature of the (simulated) biological environments. Indeed, insoluble salt formation as well as protein adsorption or the presence of amino acids can

* Corresponding author.
E-mail address: francesco.difranco@unipa.it (F. Di Franco).

https://doi.org/10.1016/j.electacta.2025.146411
Received 21 March 2025; Received in revised form 1 May 2025; Accepted 6 May 2025
Available online 6 May 2025

affect the corrosion mechanism and thus the corrosion rate. In ref. [24] the effect of ammino acids (i.e. L-cysteine) in dissolution process was investigated. In ref. [21] a detailed investigation was carried out aimed to highlight the role of biomolecules and inorganic corrosion products in affecting the corrosion behaviour of zinc with immersion tests lasting for 168 h, that allowed to estimate the corrosion rate of this metal in four different simulated physiological solutions. However, a survey of all this works still shows that there is not a general agreement on the effects of all the above cited species, and that there are not long-term immersion tests that can definitely assess the potential of Zn for bioresorbable implants [22,23,25,26].

The aim of this work is studying Zn corrosion mechanism in simulated body environments by comparing the corrosion behaviour of commercially pure zinc during immersion up to 4 weeks at 37 °C in Hanks' Balance Salt Solution (HBSS), Dulbecco's modified eagles' medium (DMEM) and DMEM with 10 % of fetal bovine serum (DMEM + 10 % FBS). While HBSS mimics only the inorganic constituent of body fluids, DMEM contains also amino acids that are present in body fluids. Addition of serum to DMEM enables to study the effect of blood proteins on the corrosion behaviour. Morphological characterizations, electrochemical tests, weight loss and ion release measurements were carried out in oxygen containing and oxygen-free environment to better understand the corrosion mechanism, (including the nature of the cathodic process) during Zn corrosion. Notably, the corrosion rate was estimated as a function of the immersion time to understand if its values can in principle match the healing process, in order to elucidate if zinc is truly promising as metallic material for biodegradable implants.

2. Materials and methods

2.1. Material preparation

Zinc samples (Goodfellow, purity >99.95 wt.%, as rolled) with a dimension of 10 × 20 mm^2 and a thickness of 0.15 mm were used. Prior to immersion test, the samples were chemically etched in 5 % wt. nitric acid aqueous solutions for 30 s and then ultrasonically cleaned in acetone and distilled water for 10 min. Samples were used after 12 h of exposure in air.

2.2. Immersion tests

Plate samples (2 cm^2) were used for immersion tests. In vitro immersion tests were carried out in different simulating physiological solutions, namely Hanks' Balance Salt Solution (HBSS), Dulbecco's modified Eagles' medium (DMEM) and DMEM with 10 % of fetal bovine serum (DMEM + 10 % FBS) up to 28 days. In Table 1 the composition of the different physiological solutions is reported. The ratio of the solution volume to the sample area was set as 20 mL/cm^2 as reported in ASTM G3–72. Samples were positioned in 50 mL sterile centrifuge tubes with 40 mL of solution and incubated at 37 °C. The test periods were 1, 3, 7, 14, 21 and 28 days respectively. In order to remove corrosion product layer, the corroded samples were firstly cleaned in 100 g/L NH_4Cl for 5 min at 70 °C according to ISO 8407:2009, and then rinsed in distilled water and dried to acquire the final weight.

2.3. Electrochemical measurements

Open circuit potential measurement (OCP), electrochemical impedance spectroscopy (EIS) and polarization curves were recorded using a Partstat 2263 (PAR). The experiments were performed at 37 °C in air and in O_2 free atmosphere (under nitrogen atmosphere) using a three-electrode configuration where a Pt net having a very high surface area was used as counter electrode and a silver/silver chloride electrode (SSC) with 3 M KCl was employed as reference electrode. OCP (Open Circuit Potential) was recorded for 30 min. EIS spectra were carried out at corresponding open circuit potential (U_{ocp}) using an amplitude of the applied sinusoidal signal of 10 mV and a frequency ranging from 100 mHz to 100 kHz. The resultant spectra were fitted via ZSimpWin software. The polarization curves were recorded with a scan rate of 5 mV s^{-1} starting from −150 mV vs. OCP and sweeping the electrode potential toward anodic direction up to 0 V vs. Ag/AgCl. Electrochemical measurements were carried out on Zn samples after immersion tests of 1, 3, 7, 14, 21 and 28 days respectively.

Table 1
Composition of different physiological solutions used expressed in g/L.

	HBSS	DMEM	DMEM+FBS
NaCl	8	6.4	6.4
KCl	0.4	0.4	0.4
$CaCl_2$	0.2	0.2	0.2
$MgCl_2$	0.2	–	–
$MgSO_4 \bullet 7H_2O$	0.06	0.2	0.2
NaH_2PO_4	0.25	–	–
Na_2HPO_4	0.06	0.124	0.124
D-Glucose	1	1	1
$Fe(NO_3)_3 \bullet H_2O$	–	0.0001	0.0001
Na-Pyruvate	–	0.11	0.11
Phenol red	–	0.015	0.015
$NaHCO_3$	0.35	3.7	3.7
L-Arginine HCl	–	0.084	0.084
L-Cysteine	–	0.048	0.048
L-Glutamine	–	0.58	0.58
L-Histidine HCl	–	0.042	0.042
L-Isoleucine	–	0.106	0.106
L-Leucine	–	0.106	0.106
L-Lysine HCl	–	0.146	0.146
L-Methionine	–	0.03	0.03
L-Phenylanine	–	0.066	0.066
L-Threonine	–	0.095	0.095
L-Tryptophan	–	0.016	0.016
L-Tyrosine	–	0.072	0.072
L-Valine	–	0.094	0.094
Glycine	–	0.03	0.03
L-Serine	–	0.042	0.042
Cholinchloride	–	0.004	0.004
Folic acid	–	0.004	0.004
Myo-Inositol	–	0.0072	0.0072
Nicotinamide	–	0.004	0.004
Da-Ca-Pantothenate	–	0.004	0.004
Pyridoxal HCl	–	0.004	0.004
Riboflavin	–	0.0004	0.0004
Thiamine-HCl	–	0.004	0.004
Fetal Bovine Serum (FBS)	–	–	10 % wt

2.4. Ion release and hydrogen evolution quantifications

To quantify the Zn ion release, PerkinElmer Inc.-Optima 2100 DV was used. For ICP–OES tests, all chemicals used were of analytical grade (purchased from Sigma Aldrich). To estimate metal release in solution, a calibration procedure was carried out with 0 (ultrapure water), 2, 5, 10, 20, 50, 100, 200, and 500 ppb for Zn standard solutions. Samplings were carried out at 1, 3, 7, 14, 21 and 28 days.

To quantify hydrogen evolution produced by cathodic reaction, zinc samples were immersed in different physiological solutions by using 250 ml glass bottles sealed with DURAN™ Bromobutyl Rubber Stopper. Hydrogen accumulated in the bottle headspace was analyzed using a 500 μl Manual Gas Tight Syringes by an HP 6890 Series GC system equipped with a Supelco GC 60/80 CarboxenTM-1000 packed column and a thermal conductivity detector.

2.5. Surface observation and corrosion product analysis

Corrosion morphologies of the immersed samples were observed using a FEI Quanta 200 FEG-SEM equipped with an EDX analyser. SEM micrographs were acquired using an accelerating voltage of 20 kV and different magnifications. The phase identification of corrosion products was performed by Micro Raman spectroscopy through a Renishaw inVia

Raman Microscope spectrometer equipped with a microprobe (50 ×) and a CCD detector with a Nd:YAG laser with a wavelength of 532 nm.

The adsorption of organic species was evaluated by employing Fourier Transform Infrared Spectroscopy (FTIR). A Spectrum One, Perkin Elmer spectrometer was used to record IR spectra on zinc samples after immersion in physiological solutions. The spectra were acquired between 4000 and 500 cm^{-1} with a resolution of 4 cm^{-1}.

3. Results and discussion

Zinc coupons were immersed at 37 °C in physiological media. For comparison, SEM micrograph with relative EDX analysis of commercially zinc sample and after chemical etching are presented in Figure S1. The surface morphology of zinc samples after immersion in different solutions are shown in Fig. 1 and S2 and the corresponding EDX analysis in Figure S3. After 1 day of immersion, SEM micrographs and EDX analysis reveal the presence of corrosion products on samples immersed in HBSS, while they are not detected on samples immersed in DMEM and DMEM + 10 % FBS (see Fig. 1a, 1d, 1g).

EDX analysis reveals the presence of Ca and P on surface immersed to HBSS for 1 day (see Fig. S3a). After 7 days of immersion, different morphologies are detected (see Fig. 1b, 1e, 1h). In particular, intergranular corrosion was observed in DMEM and corrosion attacks affecting all the surface were detected for DMEM + 10 % FBS. After 21 days of immersion, the sample exposed to HBSS is totally covered by corrosion products with lamellar shape (see Fig. 1c), prevalently composed by Mg, P and Ca (see Fig. S3c).

Raman spectra related to zinc sample after immersion in HBSS, DMEM and DMEM+FBS are reported in Fig. 2a. For sample immersed in HBSS, Raman spectra relating to three different area on the sample were registered (a, b, c). The corrosion products mainly consist of zinc-calcium phosphates. According to the active Raman modes, hopeite ($Zn_3(PO_4)_2$), scholzite ($CaZn_2(PO_4)_2$) and tarbuttite (Zn_2PO_4OH) were identified. A band for hopeite in the Raman spectrum is observed at 940 cm^{-1} and is assigned to the ν_1 PO_4 symmetric stretching mode. Other Raman bands are observed at 1150, 1059, 1000 and 995 cm^{-1} and are assigned to the ν_3 PO_4 antisymmetric stretching modes. The Raman spectrum of tarbuttite shows an intense band centred at 965 cm^{-1} assigned to the ν_1 symmetric stretching mode. The Raman spectrum of scholzite shows an intense band at 1000 cm^{-1} that is assigned to the ν_3 antisymmetric stretching modes of the PO_4. A band is observed at 923 cm^{-1} with a second band at 935 cm^{-1}. These bands are assigned to the ν_1 PO_4 symmetric stretching modes [27–29]. Raman spectra related to sample after immersion in DMEM and DMEM+FBS show dissymmetrical broad band at 570 cm^{-1} assigned to ZnO [30].

The presence of phosphate ions on the surface was confirmed by FTIR spectra in Fig. 2b Bands located at around 580 cm^{-1} and 1000 cm^{-1} correspond to PO_4^{3-} confirms the presence of phosphate-conversion layer on the surface of the sample immersed in HBSS. The band around 3300 cm^{-1} is assigned to O—H stretching vibration. In addition, FTIR spectrum for pure Zn immersed in DMEM + 10 % FBS, reported in Fig. 2b, shows the adsorption of organic species on the surface. Band located at 2900 cm^{-1} are related to stretching vibrations in C—H. Bands located at around 1650 cm^{-1}, 1550 cm^{-1}, and 1250 cm^{-1} correspond to Amide I (stretching vibrations of C═O and C—N groups), Amide II (N—H bending, C—N and the C—C stretching vibrations), and Amide III, respectively [23]. FTIR data therefore demonstrates adsorption of proteins on the surface of Zn after immersion in DMEM+FBS. The adsorption of organic species was confirmed by EDX analysis, that shows a very high percentage of carbon for sample after immersion in DMEM + 10 % FBS (see Figure S3g-i) if compared to HBSS and DMEM (see Figure S3a-f).

Fig. 3 shows mass variation and corrosion rate for different immersion times and different physiological solution. Due to the presence of large amounts of corrosion products, positive mass variation was detected for zinc in HBSS, therefore a chemical surface treatment was

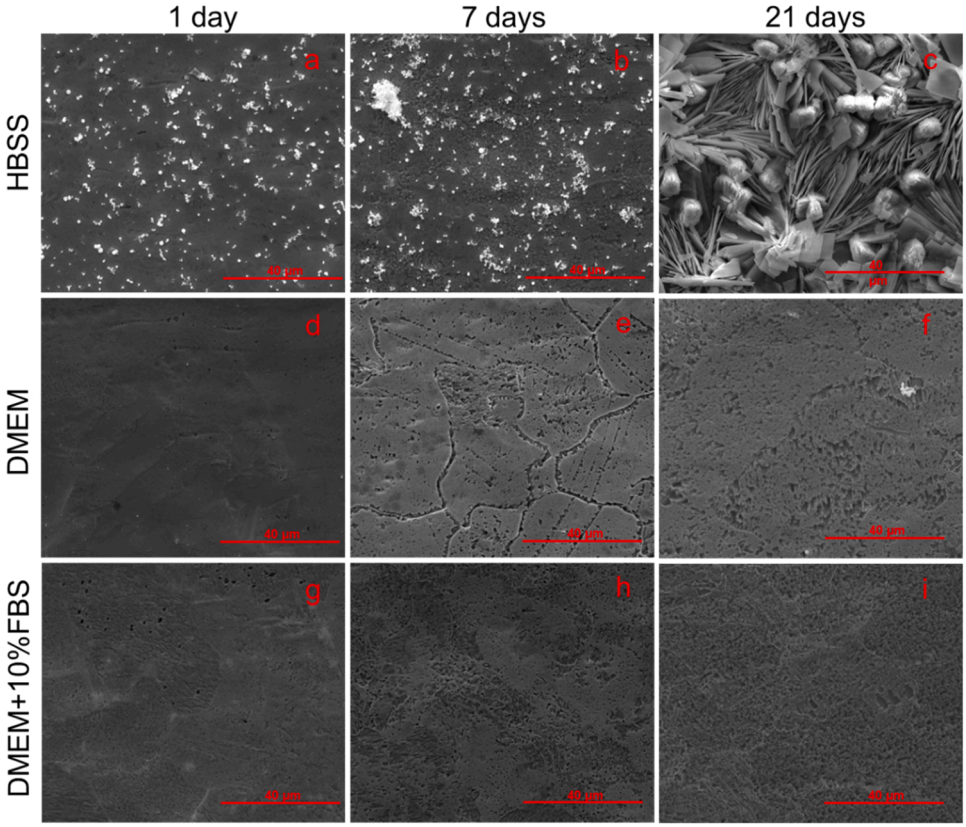

Fig. 1. SEM micrographs of Zinc samples after 1 day, 7 days and 21 days of immersion tests in HBSS, DMEM and DMEM + 10 % FBS.

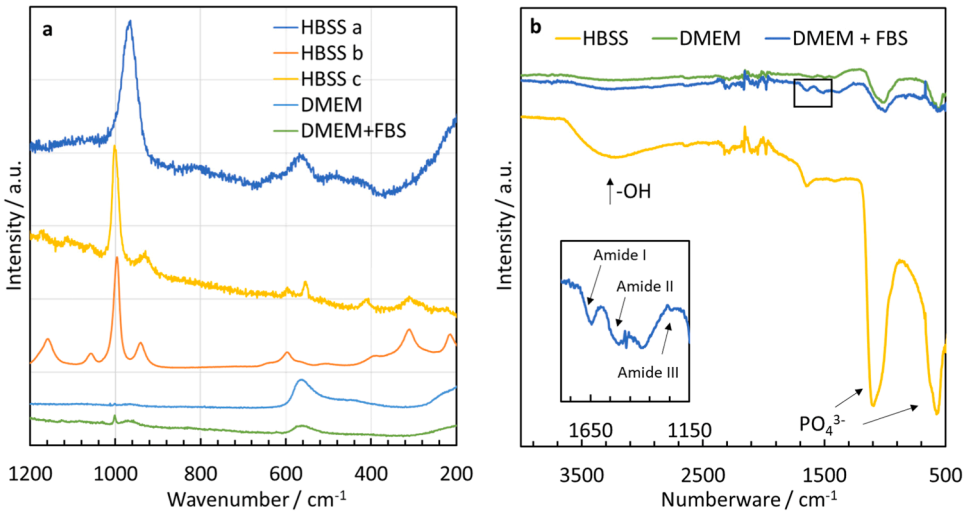

Fig. 2. a) Raman spectra and b) FT-IR spectrum related to zinc sample immersed in HBSS and DMEM with/without FBS.

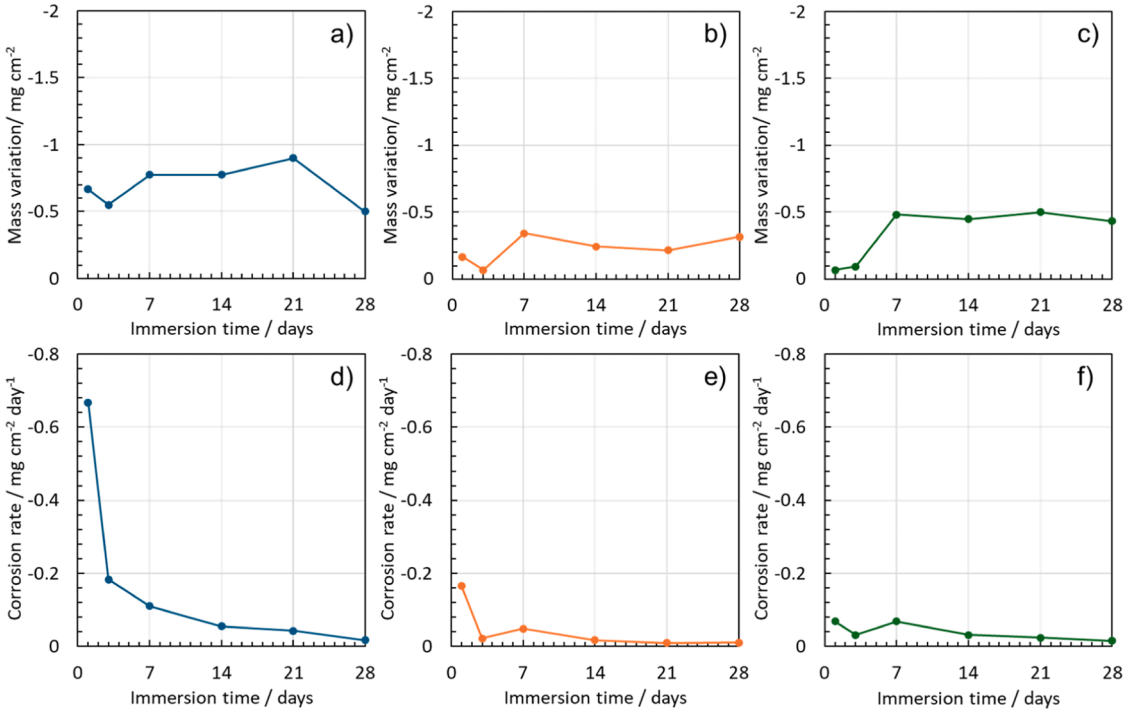

Fig. 3. Mass variation and corrosion rate of Zinc samples after different time of immersion tests in a,d) HBSS, b,e) DMEM and c,f) DMEM + FBS and after removing corrosion products.

carried out to selectively remove these compounds (see experimental section) before checking the sample weight. After the removing of corrosion products, a mass loss is measured. The weight loss is significantly higher in HBSS as compared with DMEM w/o FBS, see Fig. 3a-c. However, is interesting to note that the mass loss is almost independent on immersion time for HBSS, see Fig. 3a. Indeed, the weight loss is not affected appreciably by immersion time, thus suggesting that the corrosion products (i.e. zinc-calcium phosphates) hinder the corrosion process. Indeed, the corrosion rate in HBSS is ~ 0.7 mg cm^{-2} day^{-1} but decreases to $1.8{\cdot}10^{-2}$ mg cm^{-2} day^{-1} after 4 weeks of immersion (see Fig. 3e,f). Conversely, in the case of DMEM without and with 10 % FBS there is an increase of the weight loss after 3 days of immersion, while it does not change appreciably for longer immersion time. The corrosion rate in DMEM w/o FBS is lower if compared to HBSS and decreases to $1.3{\cdot}10^{-2}$ mg cm^{-2} day^{-1} after 4 weeks of immersion (see Fig. 3e,f). This does not mean that the corrosion process stops since the surface morphology of zinc changes according to the SEM micrographs. It is likely that the corrosion becomes more localized thus not significantly contributing to total weight losses.

Fig. 4 reports the concentration of zinc ions released during immersion in physiological media as a function of time, obtained by ICP-OES. The zinc ions released in HBSS are two orders of magnitude lower than that measured in DMEM and DMEM + 10 % FBS, as expected due to the formation of thick corrosion products layers (conversion coating) on the surface of the metal with consequent zinc ions consumption. Moreover, the values measured in DMEM and DMEM + 10 % FBS are almost independent on immersion time in agreement with the mass loss experiments.

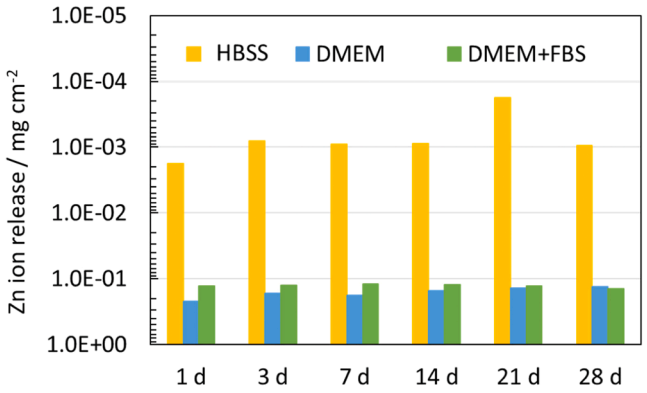

Fig. 4. Zinc ions release related to zinc samples after different time of immersion tests in HBSS, DMEM and DMEM + FBS.

In Fig. 5, EIS spectra and polarization curves, recorded in different physiological solutions with and without oxygen, are shown. For EIS spectra recorded at OCP (open circuit potential) in presence of oxygen, the overall impedance measured in physiological solutions (blue lines) is about 400 Ω cm^2 in HBSS, 1100 Ω cm^2, in DMEM and 4000 Ω cm^2 in DMEM+FBS (see Fig. 5a-c). The highest overall impedance recorded in the case of DMEM + FBS can be explained considering the protein adsorption on the sample surface. In presence of oxygen, polarization curve recorded in DMEM + FBS (see Fig. 5d-f), allows to estimate a corrosion current density, i_{corr}, lower than those recorded in HBSS and DMEM, in agreement with the results of EIS spectra. It is noteworthy to mention that a pitting potential of about –0.8 V vs. SSC can be estimated for the immersion in all physiological solutions.

To better understand the corrosion mechanism with a specific focus on the cathodic reactions, EIS spectra and polarization curves were recorded in the same physiological solutions in a O_2-free atmosphere (see yellow lines in Fig. 5).

In EIS spectra, the overall impedance measured in O_2-free atmosphere is higher than that measured in O_2-containing atmosphere in all physiological solutions. More specifically, in HBSS and DMEM the overall impedance is at least one order of magnitude higher in O_2-free atmosphere with respect to O_2-containing atmosphere, while in the case of DMEM+FBS solution it is about three times higher.

The polarization curves recorded in O_2-free atmosphere show a corrosion potential E_{corr} shifted in cathodic direction with respect to O_2-containing atmosphere, while the pitting potential is the same. The estimated corrosion current densities i_{corr} in O_2-free atmosphere are lower with respect to O_2-containing atmosphere and it is noteworthy to mention that i_{corr} does not change by changing the physiological solutions. These results allow to highlight that oxygen reduction reaction (ORR) is the main cathodic process, as has been previously reported in literature [26,31,32]. To further support this conclusion, hydrogen quantification was carried out using GC as described in the experimental section. After 28 days of immersion in all physiological solutions, the amount of evolved hydrogen is below GC detection limits, suggesting that HER as cathodic process is negligible.

In Fig. 6a-f EIS spectra in Bode representation recorded at corresponding open circuit potential, (whose values are reported in Figure S4–6) in different solutions as a function of immersion time. For zinc immersed in HBSS the overall low frequency impedance increases during the first three days of immersion (from $4{\cdot}10^2$ to $8{\cdot}10^3$ Ω cm^2), while after 1 week of immersion, it remains almost constant. This finding can be explained by the growth of the corrosion products layer, whose presence was highlighted by SEM (see Fig. 1 and S2). As evident in the Nyquist representation, since the early stage of immersion the spectra recorded in HBSS show a high frequency capacitive loop followed by a portion of a lower frequency loop. Notably, the size of the latter is not appreciably affected by the immersion time. Conversely, the high frequency capacitive loop has a diameter that increases up to 3 days of immersion, reaching a lower value for higher immersion time.

A slightly different behaviour is shown by Zn in DMEM solution. Indeed, the overall impedance at low frequency is about 1100 Ω cm^2 at the beginning of the test and changes in a narrow range for 4 weeks (i.e. between $1.4{\cdot}10^3$ and $2.4{\cdot}10^3$ Ω· cm^2). However, immersion time has a significant influence on the shape of the EIS spectrum as better evident in their Nyquist representation. Indeed, soon after immersion in DMEM the spectrum shows a high frequency capacitive loop followed by a

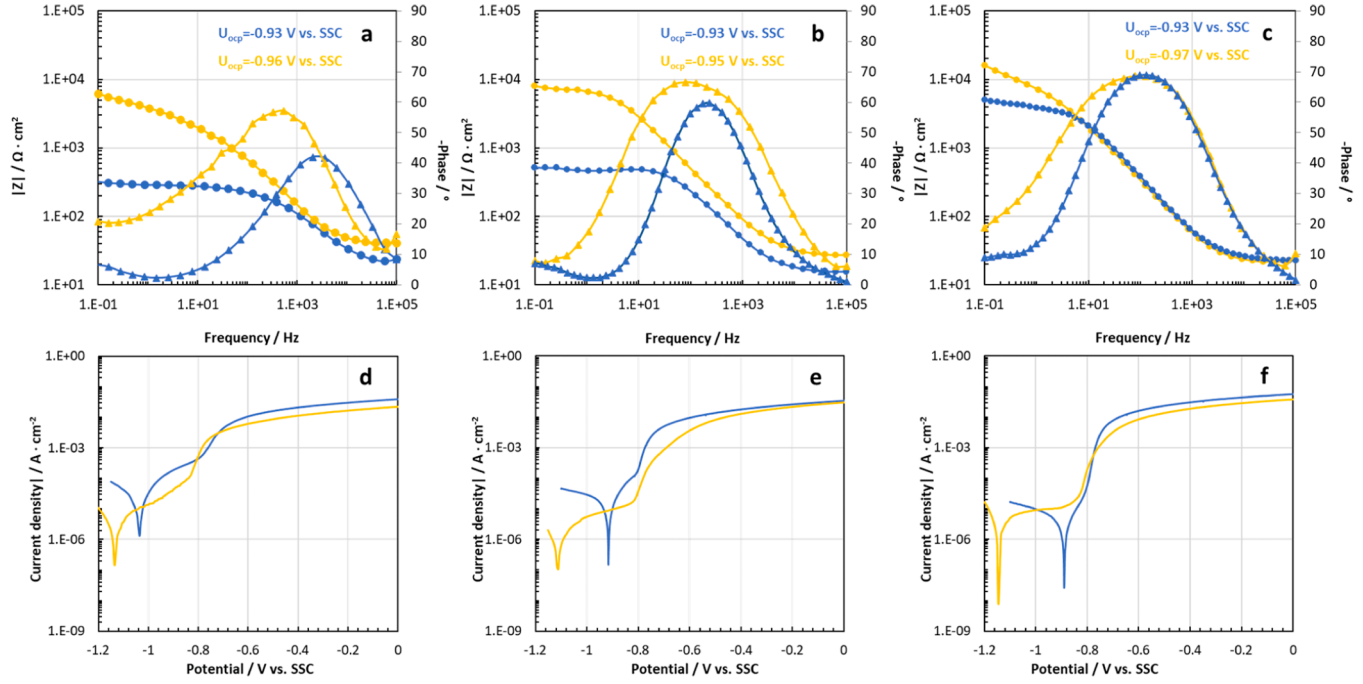

Fig. 5. EIS spectra, in Bode representation, recorded at corresponding Open Circuit Potential (U_{ocp}) and polarization curves in different solution at 37 °C with oxygen (blue lines) and without oxygen (yellow lines) after immersion of 1 h.

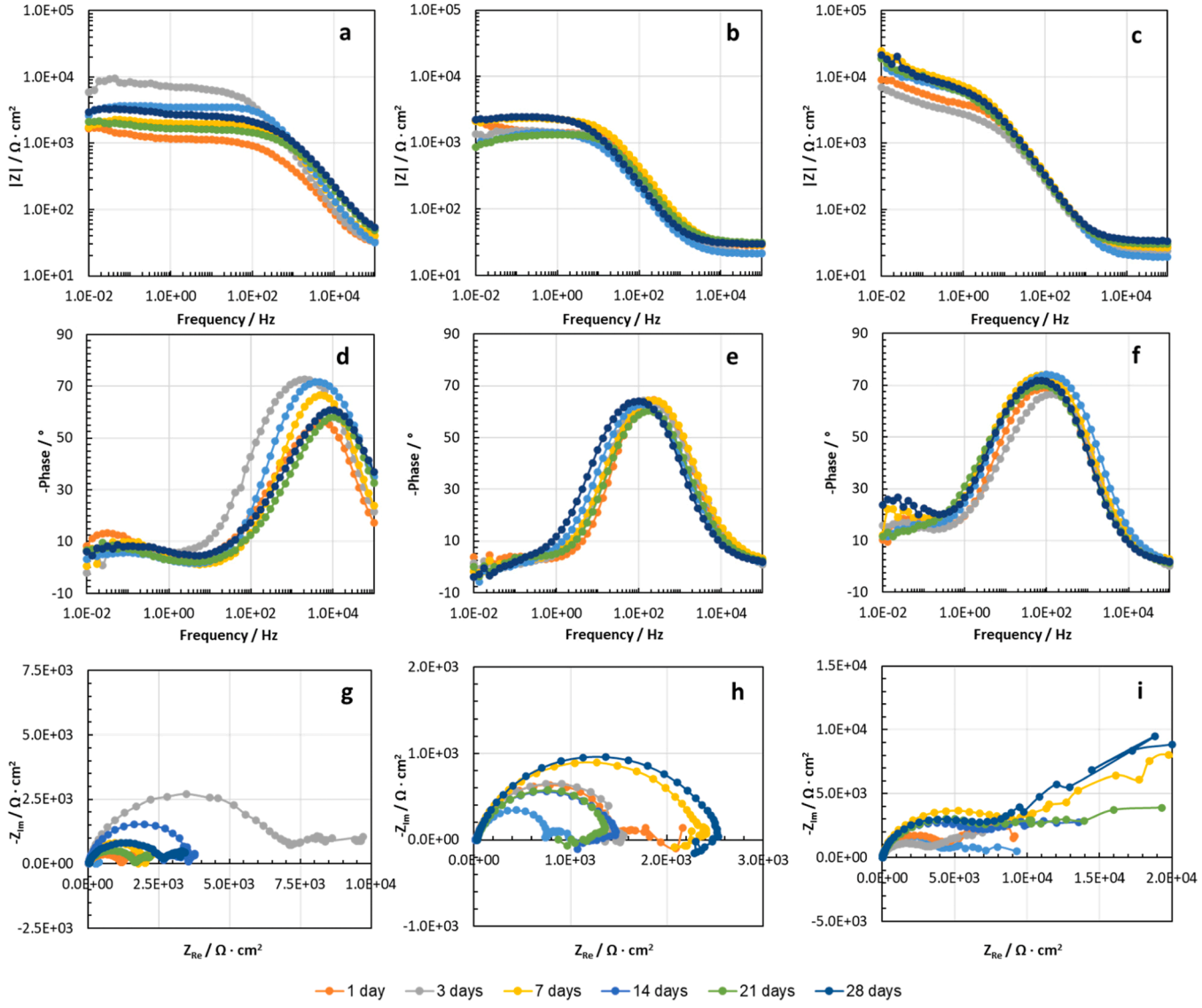

Fig. 6. EIS spectra, in Bode and Nyquist representation, recorded at corresponding Open Circuit Potential in a, d, g) HBSS, b, e, h) DMEM and c, f, i) DMEM+FBS at 37 °C after different time of immersion.

portion of a lower frequency loop, while after the first day of immersion a high-frequency capacitive loop coupled with a low-frequency inductive loop is evident. When fetal bovine serum is added to this solution, the impedance is higher and ranges between $6{\cdot}10^3$ and $1.6{\cdot}10^4$ Ω·cm^2 during the immersion up to 4 weeks. In this solution, since the early state of immersion the spectra show a high frequency capacitive loop followed by a portion of a lower frequency loop.

The EIS spectra can be rationalized in the frame of kinetic models for reaction involving the formation of an adsorbate intermediate and its successive oxidation, as detailed explained in ref. [33]. Kinetic models are superior to the use of electrical circuit analogues because the same model can account for different behaviour shown by the metal as a function of the electrolyte composition. Zinc oxidation is a two-step reaction occurring with the formation of an adsorbate intermediate (Zn^+_{ads}) and its successive oxidation to Zn^{2+} according to the following scheme (ref. [32]):

$$Zn \overset{K_1}{\rightarrow} Zn^+_{ads} + e^- \tag{1}$$

$$Zn^+_{ads} \overset{K_2}{\rightarrow} Zn^{2+} + e^- \tag{2}$$

Assuming that the adsorption of reaction intermediate Zn^+_{ads} obeys a Langmuir isotherm [32], the corresponding faradic impedance, Z_F, is a function of k_1 and k_2, of the Tafel slope for both electron transfer steps and of the surface coverage. The relation providing the equivalent impedance is:

$$Z_F^{-1} = R_t^{-1} + \frac{A}{j\omega + B} \tag{3}$$

where R_t, A and B depend on the above cited parameters. The equivalent circuit corresponding to this impedance can be different depending on kinetic parameters including the surface coverage, and can be represented by equivalent electrical circuit of Fig. 7, where adsorption impedance, Z_{ads}, is expressed as:

$$Z_{ads} = \frac{j\omega + B}{A} \tag{4}$$

When $A = 0$, the faradaic impedance reduces to $Z_F = R_t$ and the interfacial impedance only exhibits one time constant. When $A < 0$, the interfacial impedance shows two capacitive semicircles and when $A > 0$, the interfacial impedance has a high-frequency capacitive loop and low-frequency inductive loop such that the low-frequency limit for the

capacitive loop is $R_e + R_t$. For all values of A, the same expression provides the low-frequency limit for the impedance [33]. Eq. (4) is a mathematical expression that cannot be expressed as an equivalent circuit with defined passive elements when $A < 0$, while when $A > 0$ it is possible to fit the spectra with the electrical circuit reported in Fig. 7 where Z_{ads} corresponds to an inductance in series with a resistance (see table S1).

Polarization curves were also recorded after different immersion times in all physiological solutions around the open circuit potential (see Fig. 8).

The i-V curves are independent of the immersion time for DMEM, while a shift of the corrosion potential is evident for HBSS and DMEM + FBS. Notably, in the latter case a low and constant passivity current is measured in the anodic branch up to the pitting potential (−0.8 V vs. Ag/AgCl).

The results obtained considering surface morphologies characterization, electrochemical tests, mass variation test and ions release show that the corrosion mechanism for zinc immersed in different physiological solutions changes significantly. In general, the results show generalized corrosion for samples immersed in HBSS with the formation of a corrosion product layer of the surface. The samples immersed in DMEM and DMEM + 10 % FBS show different localized corrosion without the formation of a corrosion product layer and a higher zinc ion release, see Figs. 1 and 4.

The values estimated by ICP-OES are lower than that estimated by the mass losses, which is expected for HBSS due to generalized corrosion with formation of a chemical conversion coating. In the case of DMEM and DMEM+FBS this finding can be explained by precipitation phenomena that reduce the Zn^{2+} ion concentration in solution due to the formation of Zinc oxide and/or hydroxide. The cross check of mass losses and ICP ion release allows to get a reliable estimation of the zinc release rate and of the metal corrosion rate, crucial for the design of shape and thickness of biodegradable implants as a function of the composition of the electrolyte. According to the experimental findings, it seems that after 3 days of immersion, independently from the physiological solution where the tests are carried out, the mass loss and the ion release become almost constant, suggesting that the zinc corrosion rate is very low. However, the electrochemical tests and the information provided by morphological investigation as a function of time clearly show that the corrosion process is different in the investigated physiological solutions. In HBSS solution a thick zinc-calcium phosphate layer grows on the surface of the metal hindering further degradation process. Indeed, during the initial immersion, the anodic reaction is zinc dissolution and the dominant cathodic reaction is oxygen reduction. Zn^{2+} ions can react with ions such as HCO_3^- and HPO_4^- to form a less soluble corrosion product that deposits on the surface, with an increase of corrosion resistance, essentially constituted by hopeite ($Zn_3(PO_4)_2$), scholzite ($CaZn_2(PO_4)_2$) and tarbuttite (Zn_2PO_4OH). According to the measured mass losses, after the first day of immersion there is an initial mass loss in the order of 1 mg cm^{-2} corresponding to a thickness reduction of 1.4 μm. But due to the presence of these compact corrosion products, further thinning of the metal is almost negligible. When Zn is immersed in DMEM, there is no evidence of formation of this layer, due to the lower concentration of phosphate ions as well as due to complexation of Zn ions by amino acids, e.g. L-Cysteine [24]. The SEM images show the occurrence of localized corrosion but, since open circuit potential is lower that the pitting potential, it is likely that localized intergranular corrosion occurs. Despite the different corrosion behaviour, also in this solution the degradation rate becomes almost constant after the first days of immersion, probably because the mass loss is lower due to the occurrence of localized corrosion making mass changes less appreciable. For pure zinc samples this type of mechanism is not related to the presence of metallic impurities but to a crystalline type attack [34]. The real surface is not atomically flat and homogenous, but it contains in general many defects such as dislocations, vacancies and grain boundaries. The grain boundaries are locations where the atoms are less solidly bound and are preferentially attacked. The addition of 10 % of Fetal Bovine Serum (FBS) reduces intergranular attack probably due to the adsorption of proteins of the zinc surface that uniformly cover the metal. In any case, in DMEM without and with FBS the corrosion rate is even lower than that measured in HBSS and becomes negligible after the 1 – 3 days of immersion.

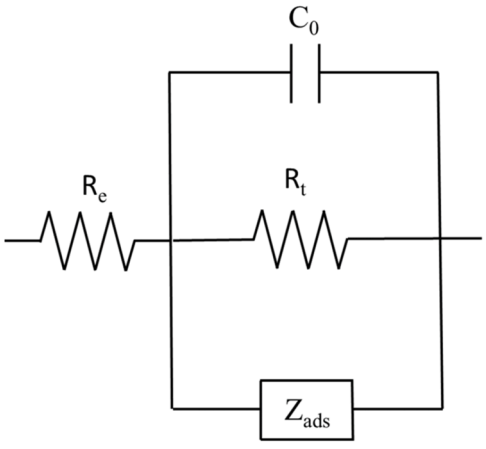

Fig. 7. Equivalent electrical circuit (EECs) used to model the electrochemical behaviour of zinc sample after immersion in different physiological solution.

The results of this study demonstrate that significantly different corrosion behaviour of pure Zn is observed in the here used three different simulated physiological solutions; not only as concern the corrosion rate but moreover also the corrosion mechanisms. Therefore, the choice of the electrolyte for studying biodegradation of Zn is crucial and should be carefully considered in view of best simulating the true biological environment. Moreover, and noteworthy, in all physiological solutions here studied, corrosion is drastically slowed down after only few days immersion, becoming almost negligible after initial burst of dissolution. This raises questions on the suitability of zinc for biodegradable implants, even before assessing its biocompatibility.

4. Conclusions

Corrosion behaviour of zinc samples was investigated in different physiological solutions, namely HBSS, DMEM and DMEM + 10 % FBS, as function of immersion time. The results obtained considering surface morphologies characterization, electrochemical tests, mass variation test and ions release, show that the corrosion mechanism for zinc samples changes significantly by changing the physiological solutions. Samples immersed in HBSS show generalized corrosion with the formation of a corrosion product layer on the surface while those immersed in DMEM and DMEM + 10 %FBS show corrosion without the formation of a corrosion product layer and consequently a higher zinc ion release. The presence of a high concentration of phosphate ions in HBSS, the chelating action towards zinc ions of amino acids in DMEM and DMEM + 10 % FBS, combined with a lower buffering action with respect to HBSS, can explain this different behaviour. Electrochemical characterizations and hydrogen quantification test reveal that HER as cathodic process in Zn corrosion is negligible.

Following immersion test in all the physiological media employed in this work up to 4 weeks, it was possible to evidence that zinc corrosion is more localized in DMEM solution with respect to HBSS, and that corrosion rate becomes very low after 14 days strong deceleration of dissolution after only few days of immersion. The presented results intend to stimulate new scientific discussion about the real possibility of using zinc as constituent material for biodegradable implants.

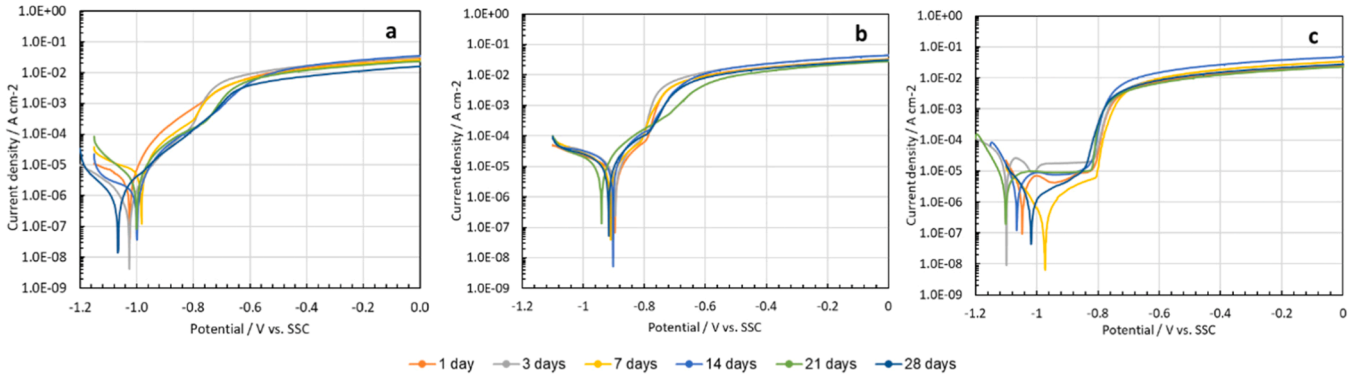

Fig. 8. Polarization curves recorded in a) HBSS, b) DMEM and c) DMEM+FBS after different time of immersion tests.

CRediT authorship contribution statement

D. Pupillo: Writing – original draft, Investigation, Formal analysis, Data curation. **F. Di Franco:** Writing – review & editing, Supervision, Formal analysis. **L. Iannucci:** Writing – review & editing, Investigation, Formal analysis, Data curation. **S. Grassini:** Writing – review & editing, Supervision, Resources. **S. Virtanen:** Writing – review & editing, Supervision, Resources. **M. Santamaria:** Writing – review & editing, Supervision, Resources, Conceptualization.

Declaration of competing interest

The authors declare that they have no known competing financial interests or personal relationships that could have appeared to influence the work reported in this paper.

Acknowledgements

M.S. and F.D.F. acknowledge the European Union (NextGeneration EU), for the support through the MUR-PNRR project SAMOTHRACE.

Supplementary materials

Supplementary material associated with this article can be found, in the online version, at doi:10.1016/j.electacta.2025.146411.

Data availability

Data will be made available on request.

References

[1] Y. Wang, C.S. Lim, C.V. Lim, M.S. Yong, E.K. Teo, L.N. Moh, In vitro degradation behavior of M1A magnesium alloy in protein-containing simulated body fluid, Mater. Sci. Eng. C 31 (2011) 579–587, https://doi.org/10.1016/j.msec.2010.11.017.

[2] X. Zhuo, Y. Wu, J. Ju, H. Liu, J. Jiang, Z. Hu, J. Bai, F. Xue, Recent progress of novel biodegradable zinc alloys: from the perspective of strengthening and toughening, J. Mater. Res. Technol. 17 (2022) 244–269, https://doi.org/10.1016/j.jmrt.2022.01.004.

[3] B. Wang, Y. Li, S. Wang, F. Jia, A. Bian, K. Wang, L. Xie, K. Yan, H. Qiao, H. Lin, J. Lan, Y. Huang, Electrodeposited dopamine/strontium-doped hydroxyapatite composite coating on pure zinc for anti-corrosion, antimicrobial and osteogenesis, Mater. Sci. Eng. C 129 (2021), https://doi.org/10.1016/j.msec.2021.112387.

[4] H. Dong, F. Lin, A.R. Boccaccini, S. Virtanen, Corrosion behavior of biodegradable metals in two different simulated physiological solutions: comparison of Mg, Zn and Fe, Corros Sci. 182 (2021), https://doi.org/10.1016/j.corsci.2021.109278.

[5] A. Zaffora, F. Di Franco, D. Virtù, F. Carfì Pavia, G. Ghersi, S. Virtanen, M. Santamaria, Tuning of the Mg alloy AZ31 anodizing process for biodegradable implants, ACS Appl. Mater. Interfaces 13 (2021) 12866–12876, https://doi.org/10.1021/acsami.0c22933.

[6] N. Li, Y. Zheng, Novel magnesium alloys developed for biomedical application: a review, J. Mater. Sci. Technol. 29 (2013) 489–502, https://doi.org/10.1016/j.jmst.2013.02.005.

[7] F. Witte, N. Hort, C. Vogt, S. Cohen, K.U. Kainer, R. Willumeit, F. Feyerabend, Degradable biomaterials based on magnesium corrosion, Curr. Opin. Solid State Mater. Sci. 12 (2008) 63–72, https://doi.org/10.1016/j.cossms.2009.04.001.

[8] F. Witte, Reprint of: the history of biodegradable magnesium implants: a review, Acta Biomater. 23 (2015) S28–S40, https://doi.org/10.1016/j.actbio.2015.07.017.

[9] A.L. Ramirez-Ledesma, P. Roncagliolo-Barrera, M.A. Alvarez-Perez, J.A. Juarez-Islas, C. Paternoster, F. Copes, D. Mantovani, Introducing novel bioabsorbable Zn–Ag–Mg alloys intended for cardiovascular applications, Mater. Today Commun. 35 (2023), https://doi.org/10.1016/j.mtcomm.2023.105544.

[10] L.M. de Andrade, C. Paternoster, P. Chevallier, S. Gambaro, P. Mengucci, D. Mantovani, Surface processing for iron-based degradable alloys: a preliminary study on the importance of acid pickling, Bioact Mater. 11 (2022) 166–180, https://doi.org/10.1016/j.bioactmat.2021.09.026.

[11] E. Mostaed, M. Sikora-Jasinska, A. Mostaed, S. Loffredo, A.G. Demir, B. Previtali, D. Mantovani, R. Beanland, M. Vedani, Novel Zn-based alloys for biodegradable stent applications: design, development and in vitro degradation, J. Mech. Behav. Biomed. Mater. 60 (2016) 581–602, https://doi.org/10.1016/j.jmbbm.2016.03.018.

[12] L. Marin de Andrade, P. Chevallier, C. Paternoster, F. Copes, D. Mantovani, Plasma immersion ion implantation of a Fe-Mn-C based steel for biomedical applications: effect of gases and treatment times on the surface properties, Key Eng. Mater. 967 (2023) 79–87, https://doi.org/10.4028/p-iy6e3n.

[13] J. Zhou, Y. Yang, R. Detsch, A.R. Boccaccini, S. Virtanen, Iron surface functionalization system - Iron oxide nanostructured arrays with polycaprolactone coatings: biodegradation, cytocompatibility, and drug release behavior, Appl. Surf. Sci. 492 (2019) 669–682, https://doi.org/10.1016/j.apsusc.2019.06.060.

[14] D. Pupillo, M.P. Bruns, L.H. Prado, F. Di Franco, D. Böhringer, A. Mazare, W. H. Goldmann, S. Virtanen, M. Santamaria, A.B. Tesler, Corrosion resistance of biodegradable zinc surfaces enhanced by UV-grafted polydimethylsiloxane coating, ACS Biomater. Sci. Eng. (2024), https://doi.org/10.1021/acsbiomaterials.4c00503.

[15] G.L. Wu, C.E. Yen, Y.S. Lin, M.L. Yeh, Evaluation of biodegradability and biocompatibility of pure zinc coated with zinc phosphate for cardiovascular stent applications, J. Med. Biol. Eng. 43 (2023) 732–740, https://doi.org/10.1007/s40846-023-00834-8.

[16] Z. Guan, C.S. Linsley, S. Pan, G. Yao, B.M. Wu, D.S. Levi, X. Li, Zn-Mg-WC nanocomposites for bioresorbable cardiovascular stents: microstructure, mechanical properties, fatigue, shelf life, and corrosion, ACS Biomater. Sci. Eng. 8 (2022) 328–339, https://doi.org/10.1021/acsbiomaterials.1c01358.

[17] J. Liu, C.S. Linsley, Y. Su, W. Abd-Elaziem, S. Pan, M. Sokoluk, A. Griebel, G. Chen, Y. Zeng, N. Murali, S. Bialo, A. Jiang, B.M. Wu, D. Zhu, X. Li, Nanoparticle-enabled Zn-0.1Mg alloy with long-term stability, refined degradation, and favorable biocompatibility for biodegradable implant devices, ACS Appl. Mater. Interfaces (2024), https://doi.org/10.1021/acsami.4c04714.

[18] J. Lin, Y. Chen, Y. Dai, X. Zhang, D. Zhang, Y. Li, C. Wen, Mechanical properties, degradation action, and biocompatibility of in situ nanoparticle-reinforced MgxZny/Zn composite prepared via roll bonding, Acta Biomater. (2025), https://doi.org/10.1016/j.actbio.2025.01.048.

[19] X. Zhuo, Y. Wu, J. Ju, H. Liu, J. Jiang, Z. Hu, J. Bai, F. Xue, Recent progress of novel biodegradable zinc alloys: from the perspective of strengthening and toughening, J. Mater. Res. Technol. 17 (2022) 244–269, https://doi.org/10.1016/j.jmrt.2022.01.004.

[20] S. Ould Mohamed, S. Gambaro, A.L. Ramirez-Ledesma, C. Paternoster, D. Mantovani, Effects of different CO2 concentrations and degradation Media on static corrosion of commercially pure zinc, Cryst. (Basel) (2023) 13, https://doi.org/10.3390/cryst13050753.

[21] X. Liu, H. Yang, Y. Liu, P. Xiong, H. Guo, H.H. Huang, Y. Zheng, Comparative studies on degradation behavior of pure zinc in various simulated body fluids, JOM 71 (2019) 1414–1425, https://doi.org/10.1007/s11837-019-03357-3.

[22] C. Wang, X. Liu, D. Mei, M. Deng, Y. Zheng, M.L. Zheludkevich, S.V. Lamaka, Local pH and oxygen concentration at the interface of Zn alloys in Tris-HCl or HEPES buffered Hanks' balanced salt solution, Corros Sci. 197 (2022), https://doi.org/10.1016/j.corsci.2021.110061.

[23] H. Dong, S. Virtanen, Influence of bovine serum albumin on biodegradation behavior of pure Zn, J. Biomed. Mater. Res. B Appl. Biomater. 110 (2022) 185–194, https://doi.org/10.1002/jbm.b.34901.
[24] V. Shkirskiy, P. Keil, H. Hintze-Bruening, F. Leroux, F. Brisset, K. Ogle, P. Volovitch, The effects of L-cysteine on the inhibition and accelerated dissolution processes of zinc metal, Corros Sci. 100 (2015) 101–112, https://doi.org/10.1016/j.corsci.2015.07.010.
[25] D. Zhu, I. Cockerill, Y. Su, Z. Zhang, J. Fu, K.W. Lee, J. Ma, C. Okpokwasili, L. Tang, Y. Zheng, Y.X. Qin, Y. Wang, Mechanical strength, biodegradation, and in vitro and in vivo biocompatibility of Zn biomaterials, ACS Appl. Mater. Interfaces 11 (2019) 6809–6819, https://doi.org/10.1021/acsami.8b20634.
[26] L. Liu, Y. Meng, A.A. Volinsky, H.J. Zhang, L.N. Wang, Influences of albumin on in vitro corrosion of pure Zn in artificial plasma, Corros Sci. 153 (2019) 341–356, https://doi.org/10.1016/j.corsci.2019.04.003.
[27] R.L. Frost, An infrared and raman spectroscopic study of natural zinc phosphates, Spectrochim Acta A Mol. Biomol. Spectrosc 60 (2004) 1439–1445, https://doi.org/10.1016/j.saa.2003.08.009.
[28] H. Zhang, Z. Chen, Q. Huang, Study of the toxicity of ZnO nanoparticles toChlorella sorokinianaunder the influence of phosphate: spectroscopic quantification, photosynthetic efficiency and gene expression analysis, Environ. Sci. Nano 7 (2020) 1431–1443, https://doi.org/10.1039/c9en01464k.
[29] A. Chennah, Y. Naciri, A. Taoufyq, B. Bakiz, L. Bazzi, F. Guinneton, S. Villain, J. R. Gavarri, A. Benlhachemi, Electrodeposited zinc phosphate hydrate electrodes for electrocatalytic applications, J. Appl. Electrochem. 49 (2019) 163–177, https://doi.org/10.1007/s10800-018-1261-8.
[30] C. Cachet, F. Ganne, S. Joiret, G. Maurin, J. Petitjean, V. Vivier, R. Wiart, EIS investigation of zinc dissolution in aerated sulphate medium. Part II, Zinc Coatings (2002).
[31] H. Fang, X. Qi, S. Zhou, S. Yang, C. Hang, Y. Tian, C. Wang, High-efficient vacuum ultraviolet-ozone assist-deposited polydopamine for poly(lactic-co-glycolic acid)-coated pure Zn toward biodegradable cardiovascular stent applications, ACS Appl. Mater. Interfaces 14 (2022) 3536–3550, https://doi.org/10.1021/acsami.1c21567.
[32] C. Cachet, F. Ganne, G. Maurin, J. Petitjean, V. Vivier, R. Wiart, EIS investigation of zinc dissolution in aerated sulfate medium, Part I: Bulk Zinc (2001). www.elsevier.com/locate/electacta.
[33] M.E. Orazem, B. Tribollet, Electrochemical impedance spectroscopy, 2008. https://doi.org/10.1002/9780470381588.
[34] D. Landolt, Corrosion and Surface Chemistry of Metals, EPFL Press, 2007.